

Growth and characterization of superconducting spinel oxide LiTi_2O_4 thin films

Rajesh V. Chopdekar ^{a,b,*}, Franklin J. Wong ^b,
Yayoi Takamura ^c, Elke Arenholz ^d, Yuri Suzuki ^b

^a*School of Applied and Engineering Physics, Cornell University, Ithaca, NY 14853*

^b*Department of Materials Science and Engineering, University of California,
Berkeley, Berkeley, CA 94720*

^c*Department of Chemical Engineering and Materials Science, University of
California, Davis, Davis, CA 95616*

^d*Advanced Light Source, Lawrence Berkeley National Laboratory, Berkeley, CA
94720*

Abstract

Epitaxial films of LiTi_2O_4 on single crystalline substrates of MgAl_2O_4 , MgO , and SrTiO_3 provide model systems to systematically explore the effects of lattice strain and microstructural disorder on the superconducting state. Lattice strain that affects bandwidth gives rise to variations in the superconducting and normal state properties. Microstructural disorder, such as antiphase boundaries that give rise to Ti network disorder, reduces the critical temperature, and Ti network disorder combined with Mg interdiffusion lead to a much more dramatic effect on the superconducting state. Surface sensitive X-ray absorption spectroscopy has identified Ti

to retain site symmetry and average valence of the bulk material regardless of film thickness.

Key words:

PACS: 74.78.-w, 61.10.Ht

1 Introduction

Spinel structure oxides offer a wealth of electronic and magnetic ground states across a broad range of temperatures. Spinel oxides with $3d$ transition metals on the octahedral sites exhibit ferromagnetism, antiferromagnetism, charge ordering, and other types of magnetic and electronic ordering depending on the average valence of the cations. However, there is only one known oxide spinel superconductor to date, LiTi_2O_4 (LTO), with a superconducting phase that persists up to 13 K. Johnston *et al.* found superconductivity in LTO as the end member of a solid solution of spinel-structure $\text{Li}_{1+x}\text{Ti}_{2-x}\text{O}_4$ ($0 \leq x \leq 0.33$).^[1,2] In the Li spinels half-integral charge exists on each of the octahedral ions due to the monovalent nature of tetrahedrally coordinated Li ions. Unlike the layered structure of superconducting cuprates, LTO has 3D connectivity of edge-sharing TiO_6 octahedra with average octahedral site valence of $d^{0.5}$ (equal amounts of Ti^{3+} and Ti^{4+}). Oxygen deficient $\text{SrTiO}_{3-\delta}$ and LTO both superconduct and both have mixed-valent Ti in octahedral coordination;^[3] however, the $\text{Ti}^{3+}/\text{Ti}^{4+}$ ratio is 1.0 in LTO while significantly more Ti^{4+} exists in $\text{SrTiO}_{3-\delta}$.

In bulk studies of primarily polycrystalline samples, there have been widely

* Corresponding author: rvc2@cornell.edu

varying normal state and superconducting properties influenced by vacancies,[4] Li content, and Ti network disorder.[5,6] Studies probing the effects of lattice strain on the superconductivity in bulk LTO have shown the application of hydrostatic pressure to enhance T_c and has been observed in both Li deficient as well as stoichiometric LTO samples.[7,8]

Epitaxial thin films of LTO are model systems for the systematic study of the role of lattice strain and microstructural disorder on superconducting properties. Epitaxial lattice strain gives rise to changes in the bandwidth that affect electron-electron correlations in many epitaxial thin film systems.[9–11] In addition, systematic variation in microstructural disorder may be obtained through the choice of substrate, giving rise to changes in film growth mode or nucleation of dislocations and other defects.[12] Such variation in microstructure can shed light on the various scattering processes that may affect its superconducting properties. Finally, the choice of substrate orientation may provide insight into either intrinsic or strain-induced anisotropic film properties.[13,14] However, to date epitaxial thin film growth has not been reported, although Inukai *et al* have synthesized polycrystalline thin films.[15,16]

In this paper, we report on the successful synthesis and superconducting and normal state characterization of epitaxial LTO thin films on single crystalline MgAl_2O_4 (MAO), MgO , and SrTiO_3 (STO) substrates. By comparing the superconducting and normal state transport properties we are able to identify the role of lattice strain, Ti network disorder and stoichiometry on superconductivity. For example, misregistry and disorder at grain boundaries emerge in films grown on STO and MgO due to coalescence of spinel LTO grains that possess twice the unit cell dimension of the underlying substrate; such defects are termed antiphase boundaries. Antiphase boundary disorder has been

well-characterized in spinel films grown on MgO substrates via transmission electron microscopy analysis.[17,18] These defects disrupt Ti-O-Ti octahedral bond ordering in an analogous manner to the disruption of Fe-O-Fe bond ordering in Fe_3O_4 ,[19,20] and such Ti network disorder would influence carrier transport in LTO films. On the other hand, Mg interdiffusion combined with antiphase boundary-related Ti disorder has a much larger effect on both normal state and superconducting properties. Surface sensitive X-ray absorption (XA) spectroscopy has identified Ti to retain site symmetry and average valence of the bulk material. Together these results demonstrate the robustness of superconductivity in LTO to lattice strain and microstructural defects.

2 Experimental Methods

We have chosen to study epitaxial LTO films on MAO, MgO, and STO substrates. A previous report indicated that diffusion of Mg into LTO could suppress the superconducting phase,[21] and in this case the source of Mg would be interdiffusion from the underlying substrate at the film-substrate interface. STO substrates were used to confirm the trends found in studies on MAO substrates as independent of the presence of Mg. LTO films on MAO and STO show minimal interdiffusion at the film-substrate interface while there is significant Mg diffusion on MgO substrates. Furthermore, each of these substrates placed the film under differing amounts of lattice strain through epitaxy.

Nominally stoichiometric LTO material prepared by solid-state reaction yields a lattice parameter of 0.8405 nm by powder X-ray diffraction analysis.[22] Films on MgO (lattice constant $a = 0.4211$ nm, film-substrate mismatch $f = +0.21$ %) are under slight tension, while films on MAO ($a = 0.8083$ nm, $f =$

-3.82 %) are under compressive strain. Since other spinels have been shown to grow epitaxially on perovskite-structure substrates,[23,24] LTO films were also grown on perovskite STO ($a = 0.3905$ nm, $f = -7.07$ %). The perovskite substrate promoted the growth of the spinel superconducting phase in spite of the high compressive strain and anti-phase boundaries due to the unit cell of LTO being twice a perovskite unit cell.

Epitaxial thin films of the normal spinel structure oxide LTO were deposited via pulsed laser deposition on single crystalline (001)-oriented MgO, (001), (111) and (110)-oriented MAO, and TiO₂-terminated (001) and (110)-oriented STO with thickness ranging from 5 nm to 1 μ m. Stability issues in air and the so-called ‘aging effect’ were seen in previous samples of stoichiometric LTO.[25,26] Therefore the commercial target (Praxair Surface Technologies) was a mixture of the stable phases ramsdellite lithium titanium oxide (Li₂Ti₃O₇)[27,28] and rutile titanium oxide (TiO₂) to achieve a Li:Ti ratio of 1:2. Powder X-ray diffraction confirms the presence of these oxides in the target powder but no spinel-type phase reflections were found.

Substrate temperatures were held at 450-600 °C in a vacuum of better than 5×10^{-6} Torr to promote growth of the superconducting phase. Smooth films with low particulate density (less than 0.05 particles/ μ m²) were produced with laser fluence of 1-2 J/cm² and a repetition rate of 3 Hz, resulting in a deposition rate of approximately 0.03 nm per pulse.

Rutherford Backscattering Spectrometry (RBS) was used to evaluate both film thickness and composition. However, quantitative analysis of low-Z ions such as Li and O is difficult, so only Ti atom density and uniformity were obtained using this technique. X-ray diffraction both in θ - 2θ and 4-circle mode us-

ing Siemens D5000 diffractometers assessed film crystallinity and orientation. Cross sectional high-resolution transmission electron microscopy (HRTEM) was performed on a Philips CM300 in order to examine the structure of the film-substrate interface.

Soft XA spectroscopy on the Ti $L_{2,3}$ and O K edges of LTO films was performed at beamlines 4.0.2 [29] and 6.3.1 [30] of the Advanced Light Source. X-ray absorption spectra for LTO films of thickness 15-300 nm were taken at room temperature in both normal and grazing incidences with a probing depth of 2-5 nm. The lateral dimensions of the X-ray interaction area are much larger than the electron escape depth vertically, thus the measured signal averages over a large number of intragrain volume as well as grain boundaries.

Normal and superconducting-state magnetic properties were measured in a Quantum Design superconducting quantum interference device (SQUID) magnetometer. Magnetization measurements were performed with DC field applied both in the plane and out of the plane of the sample. Transport properties were measured in a Quantum Design physical property measurement system (PPMS) modified with a Keithley 236 source-measure unit and HP3488A switching matrix.

3 Structure

Structural analysis indicated that films on all substrates were single-phase and single orientation spinel composition. X-ray diffraction in θ - 2θ geometry showed spinel phase reflections that were epitaxially matched to the single crystal substrate. No reflections from constituent phases from the target or

polymorphs of TiO_2 were observed. Films on MAO and STO under compressive strain exhibited elongation of the out-of-plane lattice parameter. Reciprocal lattice mapping of the film 444 reflection on (110) STO showed almost full relaxation of the film to bulk lattice parameters for film thickness greater than 100 nm, but only partial relaxation below 100 nm. Careful X-ray diffraction measurements indicated that the lattice parameters of LTO were elongated along the out-of-plane direction with approximately 2% elongation from bulk for a 22 nm thick film on (001) MAO. Films on MgO had reflections which overlay the substrate reflections to within the experimental resolution of the diffractometer. This result indicates that the films are under slight tension and show very little contraction of the out-of-plane lattice parameter. In-plane (ϕ) x-ray diffraction scans were performed to measure the in-plane epitaxy of the samples, with clear signs of cube-on-cube epitaxial growth of the spinel on perovskite STO substrates (Figure 1, top).

Atomic force microscopy (AFM) indicated the low lattice mismatch between LTO and MgO gave rise to smooth films with an RMS roughness of 0.444 nm (or approximately half of a spinel unit cell) for a 100 nm thick film on (001) MgO. However, rougher film morphology was seen on (001) MAO substrates, with 1.6-2.6 nm RMS roughness for films of similar thickness. Films on (001) STO had comparable roughness to those on (001) MAO, and film grain size for both substrates at a deposition temperature of 450 °C or 600 °C was on average 100 nm. The rougher surface morphology when compared with films on (001) MgO was attributed to the larger epitaxial lattice mismatch and the accompanying full lattice relaxation. Films on (110)-oriented STO and MAO substrates had elongated grains with an aspect ratio of 2:1 favoring the $[\bar{1}\bar{1}0]$ in-plane axis as the fast-growth direction, as well as increased out-of-

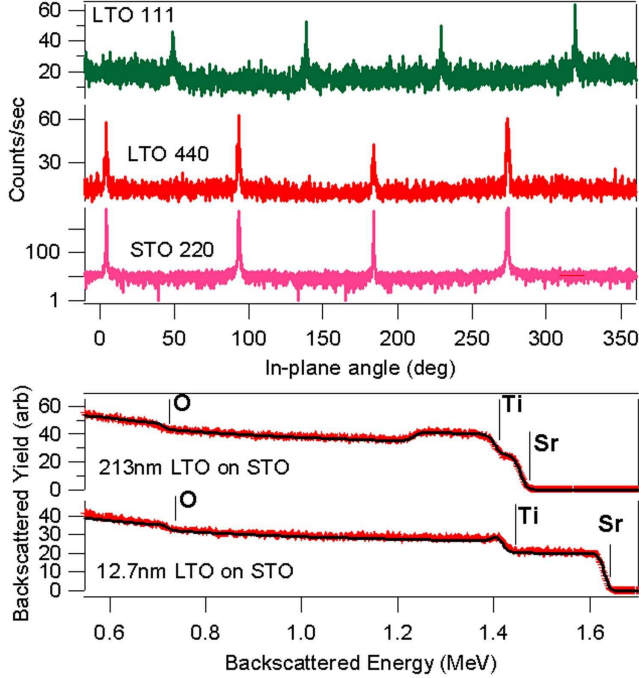


Fig. 1. (Color online) Top - In-plane (ϕ) x-ray diffraction scan of LTO 111 and 440 reflections as well as STO 220 reflections. Note that the STO reflection is on a logarithmic scale while the LTO reflections are on linear scales. Bottom - RBS experimental and simulated (solid line) spectra for LTO/STO films of 12.7 and 218 nm thickness, with vertical lines indicating the elemental thresholds for O, Ti, and Sr.

plane roughness compared to (001)-oriented films. No measurable anisotropy or roughening compared to (001) films was measured on films grown on (111)-oriented MAO, though the average grain size of 30 nm was smaller than grain sizes of (110) films with comparable thickness.

RBS analysis enabled us to probe the degree of interdiffusion of species at the film-substrate interface. Because of the difficulty in analyzing low Z ions such as Li and O, we focused on analyzing the uniformity of the atomic density of Ti from the LTO as well as the atomic species from the respective substrates. RBS analysis confirmed the interdiffusion of Mg into the LTO films deposited

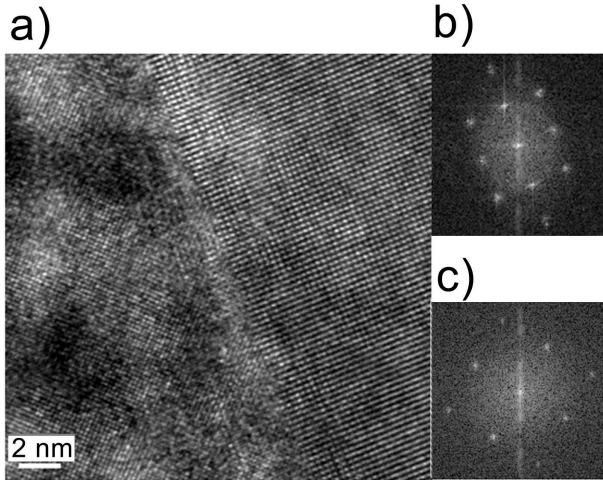


Fig. 2. (a) HRTEM image of the film-substrate interface of a (110) LTO/STO sample, with the STO substrate on the right of the micrograph. (b) Fourier transform of the combined image. (c) Fourier transform of an LTO-only area of the sample.

at 600 °C from MgO substrates with an approximate ratio of Mg to Ti of 0.25:2 assuming a uniform film stoichiometry. But no measurable interdiffusion was detected for films on STO or MAO substrates to within the 5% accuracy of the measurement (Figure 1, bottom).

HRTEM micrographs of a (110) LTO/STO sample along the [001] zone axis were taken to examine the non-isostructural spinel-perovskite interface (Figure 2, (a)). Fourier transforms of the film-substrate interface area (Figure 2(b)) as compared to film-only areas (Figure 2(c)) confirm epitaxial growth of the film on the STO substrate. The clear presence of well-defined film lattice fringes in multiple areas of the TEM sample corroborates the single phase and single orientation nature of the sample from the x-ray diffraction measurements. However, low angle grain boundaries can be seen on the film side of the interface as areas of differing contrast. Thus we must be aware of the influence of such grain boundary defects on resistivity and magnetization.

4 X-ray Absorption Spectroscopy

In order to probe the cation environment and its effect on the observation of superconductivity, surface sensitive soft XA spectroscopy was performed at the Ti $L_{2,3}$ and O K absorption edges on films of varying thickness below 500 nm to determine the Ti ion environment. Spectra have been aligned to the first sharp feature at each absorption edge: 455 eV for the Ti L_{3a} peak (Figure 3) and 530 eV for the first O K edge peak (Figure 4). Unlike heavier $3d$ transition metals like Fe with two dominant features representing the L_2 and L_3 edges, the Ti L_3 and L_2 absorption features are split into qualitatively t_{2g} -like (labeled as L_{3a} and L_{2a}) and e_g -like (L_{3b} and L_{2b}) sub-peaks. Crystal fields have a large effect on the relative intensity of each of these peaks for the case of Ti^{4+} in different environments.[31,32] Since bulk LTO has an equal number of Ti^{3+} and Ti^{4+} in octahedral environments, one would expect a spectrum similar to mixed-valence octahedral Ti such as in $La_{1-y}Sr_yTiO_3$. [33] Comparison of the STO Ti^{4+} -only spectrum in Figure 3(a) to LTO spectra displayed in Fig. 3(c)-(e) shows that LTO spectra have an increase in spectral weight at a 454 eV pre-peak features at the expense of L_{3a} intensity. Moreover, a merging of the L_{2a} and L_{2b} peaks is observed. This trend is also seen in the $y=0.4$ and $y=0.6$ spectra from Abbate *et al.*'s study on $La_{1-y}Sr_yTiO_3$. [33]

Ra *et al.* [34] examined powders of stoichiometric and Li-excess $Li_{1+x}Ti_{2-x}O_4$ and found qualitatively similar Ti $L_{2,3}$ lineshapes for $0 \leq x \leq 0.33$. Following their analysis, Lorentzian fits were made simultaneously to the pre-edge feature at 454 eV as well as each of the L_{3a} , L_{3b} , L_{2a} , and L_{2b} peaks. The ratio of L_{3a} to L_{3b} peak areas was approximately 0.14 for LTO on MgO and MAO, and showed a trend of increasing L_{3a} contribution for films on STO. This result

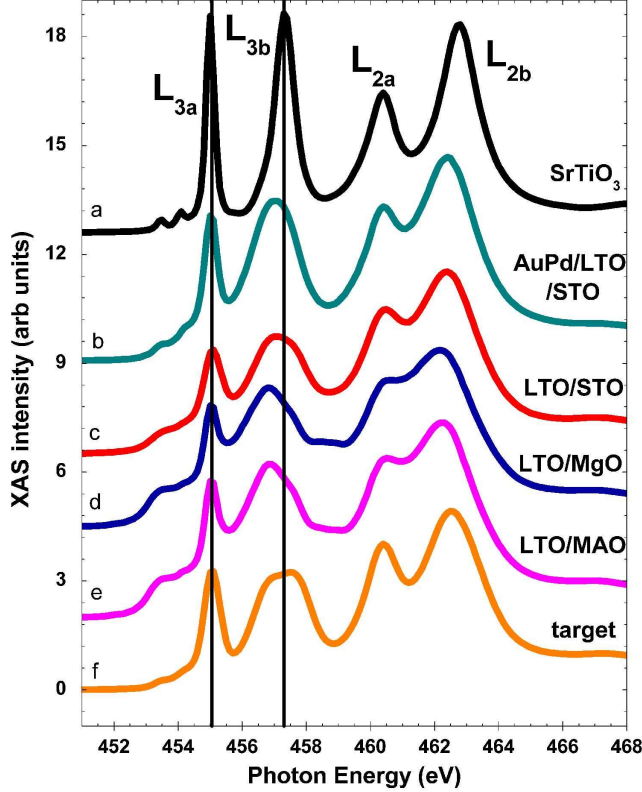


Fig. 3. (Color online) Normal-incidence Ti $L_{2,3}$ absorption edge spectra for LTO films on various substrates: (b) 3 nm AuPd / LTO on (001)STO, (c) LTO on (001)STO, (d) LTO on (001)MgO, and (e) LTO on (001)MAO, as well as spectra from (a) a bare STO wafer and (f) the pressed powder target mixture as sources of Ti^{4+} -only compounds.

suggests that the surface of films on STO have slightly more Ti^{4+} character than similar films on MgO or MAO. Samples on STO capped with 3 nm AuPd deposited in-situ at 400 °C showed similar spectra to uncapped samples, suggesting that the more Ti^{4+} -like spectrum is intrinsic to the surface and interface of as-deposited LTO films on STO.

The O K edge features may be divided into two regions: two low-energy peaks at 530 eV and 532.5 eV that show strong hybridization between O $2p$ and Ti $3d$ states, and a broader region between 536-548 eV exhibiting mixing of Ti $4sp$

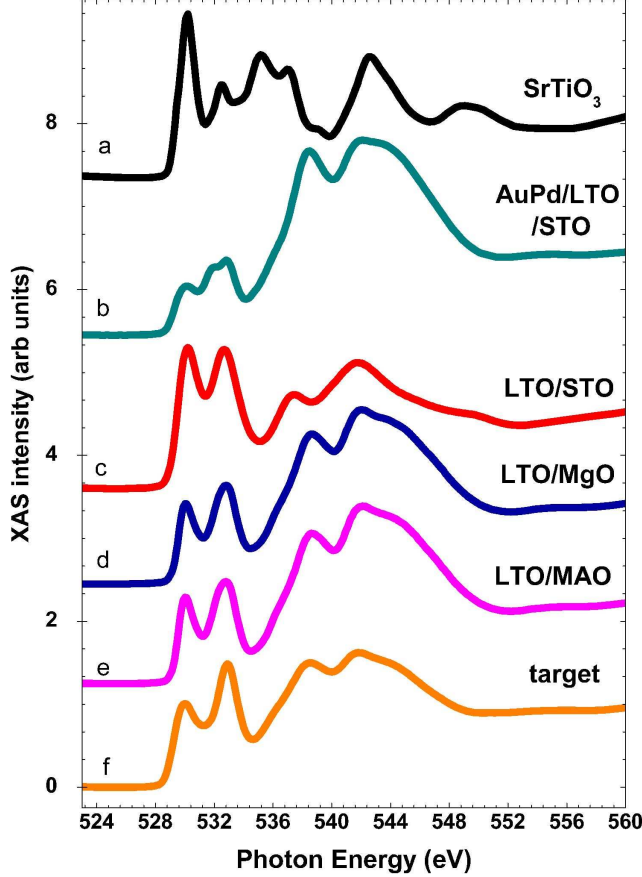


Fig. 4. (Color online) O K absorption edge spectra for LTO films on various substrates as well as reference spectra as described in Figure 3.

and O $2p$ states.[31] The lower-energy peaks for the various samples resemble the spectrum from the target material due to similar Ti-O hybridization with the intensity for the two peaks equal in magnitude and insensitive to film thickness from 15 nm to 87 nm on STO.

Comparison of our data with the spectra from Ra *et al.* confirm that the surface material is close to target stoichiometry as-deposited for all films. All samples shown in Figures 3 and 4 show little difference in XA spectra lineshape between grazing and normal incidence measurements, thus suggesting that the surface has similar characteristics to the rest of the film. Therefore the variations in transport properties for different samples described below cannot

be attributed to variations in Ti average valence, Ti site symmetry or Li deficiency and hence Ti network disorder.

Although XA spectra are very sensitive to site symmetry for isovalent compounds such as rutile and anatase TiO_2 ,^[32] no clear differences between XA spectra is observed as a function of LTO layer thickness. Thick and relaxed films on MAO, MgO and STO substrates also have similar features to the thin films on STO, indicating that the surface monolayers do not change substantially post-deposition as a function of substrate, and the XA surface measurement is insensitive to the presence of antiphase boundary disorder.

XA spectra at the Mg K edge of 100 nm thick as-deposited films on MgO substrates (peak to background of 1.25:1) confirms interface Mg diffusing from the substrate into the film during growth. Similarity of the aforementioned spectra to normal spinel MAO Mg K edge spectra^[35] confirms that the interdiffused Mg substitutes primarily into tetrahedrally coordinated sites. However, a comparable as-deposited 100 nm thick LTO film on MAO shows little Mg at the surface, with a peak to background of approximately 1.01:1 for the Mg K edge.

5 Magnetism

The magnetic response of LTO films was measured on all substrates and found to be comparable to LTO bulk single crystals, polycrystalline pellets, and powder samples. Zero-field cooled samples at 1.8 K show diamagnetic shielding with low applied fields. A linear extrapolation at low applied fields for the data presented in Figure 5 (a) yielded a typical lower critical field H_{c1} of 46 ± 3 Oe at which point the diamagnetic response deviated from linearity by 1 %. We

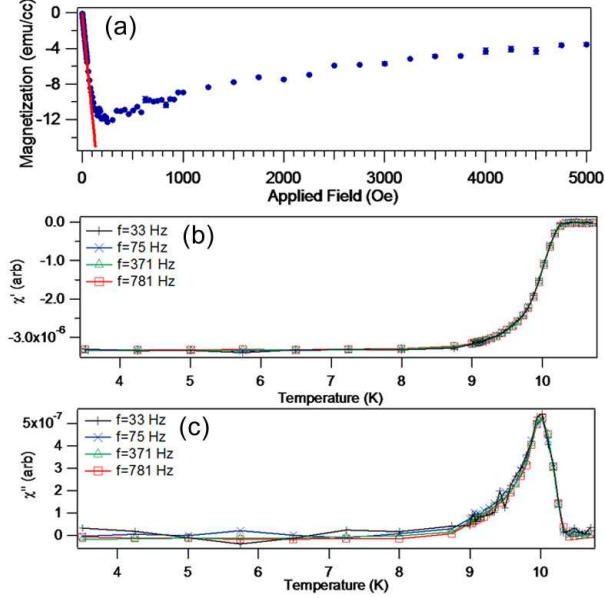


Fig. 5. (Color online) (a) Low-field diamagnetic response at 1.8 K of a zero-field cooled 350 nm LTO film on (001)MAO with magnetic field in the plane of the sample. Deviation from linearity takes place at 46 ± 3 Oe. (b) Zero-DC field in-phase magnetic susceptibility as a function of temperature for a 300 nm LTO film on (110)MAO with excitation field $H_{ac} = 14$ Oe. (c) Out-of-phase susceptibility of sample in (b).

assume the relation $(H_{c1}H_{c2})^{0.5} \approx H_c$, with H_c as the thermodynamic critical field for LTO, and obtain an upper critical field H_{c2} of approximately 20 T using Sun *et al.*'s value for $H_c = 0.327$ T.[36] As discussed below, we may extract the upper critical field from transport measurements, and such values yield $H_c \approx 0.3$ T in good agreement with Sun *et al.*'s results.

AC susceptibility has been used to characterize superconducting samples to determine the fraction of superconducting phase as a function of DC magnetic field, AC excitation field and temperature.[37] One can model a polycrystalline sample as a collection of superconducting grains with weak links representing grain boundaries. Thus the intragrain and the intergrain AC response may be

separated and individually evaluated. However, as a function of frequency, no secondary peak is observed in the AC response to within the resolution of the measurement as shown in Figure 5. We conclude that the presence of low-angle grain boundaries as determined by TEM does not seem to adversely affect the LTO film response and that the superconducting material is strongly coupled across such low angle grain boundaries. In spite of the presence of both low-angle grain boundaries and antiphase boundaries in the LTO samples on STO, the measured in and out-of-phase AC response matches the DC temperature-dependent magnetization.

6 Transport

In order to probe the effects of lattice strain and microstructural disorder on the superconducting transition, we performed resistivity measurements on our LTO films. In particular, we discuss the normal state resistivity values, resistive transition temperatures and widths, the upper critical field, and the Ginzburg-Landau coherence length-mean free path product as a function of substrate.

The normal-state resistivities versus temperature for nominally stoichiometric films on MAO (e.g. Figure 6) and STO deposited at 600 °C are comparable to that of polycrystalline thin films[15] and polycrystalline bulk samples[38] despite the presence of large compressive epitaxial strains. The film on (001) MAO described in Figure 6 as well as a film of comparable thickness on (001) STO both have a resistivity of $1.2 \times 10^{-3} \Omega \cdot \text{cm}$ at 12K. The similarity in magnitude of normal-state resistivity suggests that the presence of antiphase boundaries, and hence Ti network disorder, in films on STO does not have a signifi-

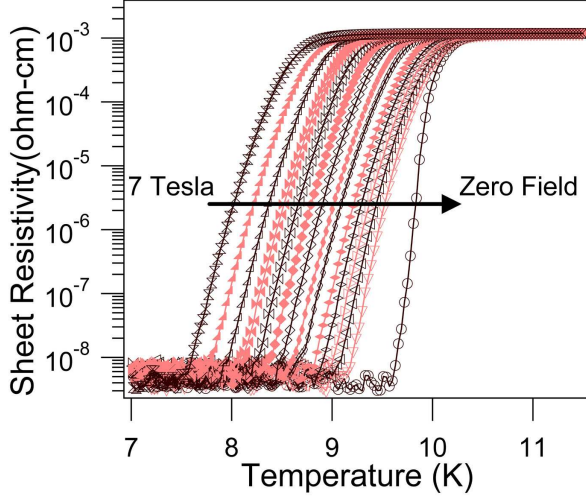


Fig. 6. (Color online) Zero-field cooled field-dependent resistivity taken on warming as a function of temperature of a 60 nm film on (001)MAO in the temperature regime around its superconducting transition. Measurements were taken with field applied out of plane at every 0.5 T from 7 T to zero field, with bold black lines indicating data at 1 T intervals.

cant effect on the normal state transport in such LTO films. In contrast, films on MgO were found to have an order of magnitude greater normal-state resistivity despite having minimal epitaxial strain and much smoother film morphology compared to films on STO or MAO. The significantly larger normal state resistivity values suggest that partial Mg^{2+} interdiffusion into octahedral sublattice sites[21,22,39] at the 600 °C deposition temperature, coupled with antiphase boundary-related Ti network disorder[6], give rise to greater scattering in the normal state. A lower deposition temperature of 450 °C yielded films with higher residual resistivity for all substrates, though superconducting transitions for films on MAO and STO remained at approximately 10 K. These results suggest that the higher residual resistivity is associated with the grain boundaries.

Figure 7 shows a summary of the resistive transition temperatures and widths

measured for LTO films of varying thicknesses grown on different substrates and substrate orientations. Mirroring the trend observed with the normal state resistivity values, the films grown on (001) MAO and STO display similar behavior with a sharp zero field transition width (for 10% to 90% of normal state resistivity at 15 K) and transition temperature near 10.8 K. Nominally unstrained films on (001) MgO show a sharper zero field transition width of 0.3 K but with transition temperatures depressed to 6.9-9 K. The lower transition temperatures on MgO substrates, in contrast to those on MAO and STO substrates, can result from more significant Mg interdiffusion into the LTO film.[22] LTO films of 150 nm thickness on (110) or (111)-oriented MAO substrates show broader transition widths of up to 1.5 K which may be linked to smaller grain size seen in the AFM scans. The increased number of non-superconducting grain boundaries in such samples could dominate the resistivity measurement, or the intragrain volumes themselves may be off-stoichiometry. Similar broadening of transition widths without significant degradation of the transition temperature were seen in powder pellets of LTO[40] as well as artificial $\text{YBa}_2\text{Cu}_3\text{O}_7$ superlattices.[41] The broadening in the aforementioned studies was not due to intrinsic properties of the superconducting regions but instead the boundary regions with the non-superconducting material. Since the LTO film transition temperature remains unchanged as a function of orientation for the 150 nm thick LTO films in Figure 7, grain boundaries rather than whole-film non-stoichiometry is the source of the transition broadening. If the grain boundary resistance in LTO films is a significant fraction of the measured normal-state resistance, careful analysis must be performed to separate intrinsic LTO properties from boundary effects. Finally, films on STO have comparable transition temperatures to films on MAO, implying that antiphase boundaries have little effect on the

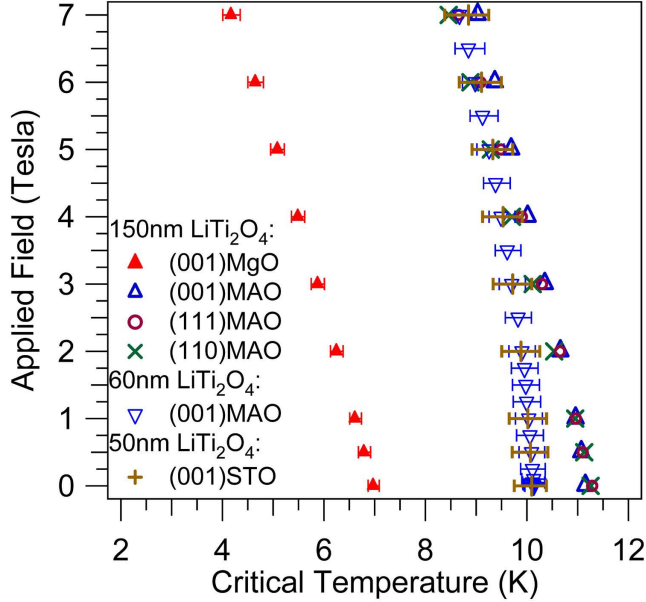


Fig. 7. (Color online) Critical temperature versus applied field for 50 nm, 60 nm and 150 nm LTO films on various substrates with magnetic field applied out of the plane of the sample. The horizontal error bars indicate the superconducting transition temperature width (10%-90% of the resistivity at 15 K).

magnitude of the critical temperature.

A closer look at the upper critical field and Ginzburg-Landau coherence length-mean free path product of LTO thin films on different substrates indicates the presence of a disordered phase either at the surface or film-substrate interface in thinner LTO samples. Using the Werthamer, Helfand and Hohenberg [42] (WHH) model for a type II superconductor in the dirty limit, we can estimate the upper critical field (H_{c2}) from the low-field slope of the critical temperature as a function of applied magnetic field. The extracted $H_{c2}(T=0\text{ K})$ values ranged from 15.5-19.5 T for eighteen samples deposited on MAO and STO. The coherence length $\xi(T = 0\text{ K})$ may be estimated from the Ginzburg-Landau formula $H_{c2} = \Phi_0/2\pi\xi^2$ as 4.1-4.6 nm which is consistent with bulk values. Foner and McNiff[43] found that in spite of different starting compositions of

Li_{2.6}Ti_{2-z}O₄, T_c values were uniformly 12 K for stoichiometry deviations in the range of $-0.7 < z < 0.5$. However, strong variations were observed in the quantities $(dH_{c2}/dT)_{T=T_c}$, the zero-field slope of the H_{c2} vs T_c curve, and λ_{so} , the spin-orbit scattering parameter. In analogy, the T_c of films on MAO and STO for a given thickness is suppressed in thinner films to an average T_c of 10.8 ± 0.5 K compared to 600 nm thick films with an average T_c of 11.3 ± 0.3 K. Thinner films such as the 60 nm film on (001) MAO or 50 nm film on (001) STO in Figure 7 show a field dependence with suppressed critical temperatures in zero field, though in high field their behavior approaches those of thicker films. The films on MgO had a suppressed critical temperature but fit very well to the universal WHH curve when the reduced field $h_{c2} = H_{c2}(T)/[T_c(H = 0) \cdot (dH_{c2}/dT)_{T=T_c}]$ is plotted as a function of reduced critical temperature $t = T_c(H)/T_c(H = 0)$.

The Ginzburg-Landau coherence length-mean free path product $\xi_0 l$ may also be extracted from the transport data using the dirty-limit formula

$$\xi(T) = 0.855 \left(\frac{\xi_0 l}{1 - T/T_c} \right)^{\frac{1}{2}} \quad (1)$$

For the resistive transitions plotted in Figure 7, $\xi_0 l$ for the 150 nm thick films is 14 nm^2 and this value is consistent with crystals at 5% or closer in composition to the stoichiometric LiTi₂O₄ phase.[36,38] However, the 50 nm and 60 nm films on both MAO and STO have $\xi_0 l$ values of 8 nm^2 , suggesting that deviations from bulk-like behavior at either the surface or the film-substrate interface dominate at these thicknesses. Examination of the film-substrate interface in the HRTEM micrographs does not reveal an interface layer, and there is no clear thickness dependence of the surface layer as measured by XA spectroscopy. Thus epitaxial strain may cause thin film properties to deviate

from bulk, while thick and relaxed film properties are closer to those of bulk LTO.

7 Conclusion

Epitaxial films of the spinel superconductor LTO were grown on a variety of substrates to explore the effects of strain and microstructure on measured normal state and superconducting properties. Transport and magnetic measurements were consistent with bulk samples with an average critical temperature of 10.8 K and sharp transition width for films deposited on (001) MAO and STO. The surface properties of films on a variety of substrates were identical as measured by soft X-ray absorption spectroscopy on the Ti L_{2,3} edges. Antiphase boundaries have little if any contribution to the normal and superconducting transport as well as magnetic properties of LTO films deposited on perovskite STO substrates. By contrast, the interface Mg interdiffusion combined with antiphase boundaries in LTO films on MgO substrates gives rise to suppressed critical temperature accompanied by higher than bulk normal-state resistivity values. Together these results indicate the robustness of the superconducting state of LTO to lattice strain and microstructural disorder.

8 Acknowledgments

The authors thank Prof. A. Stacy (UC Berkeley, Chemistry) for the use of her θ - 2θ diffractometer and K. M. Yu (Lawrence Berkeley Lab, Materials Science Division) for taking RBS spectra. RVC would like to thank J.S. Bettinger and B. B. Nelson-Cheeseman for assistance in collecting XA spectra, and Y. Mat-

sushita, I.R. Fisher and M.R. Beasley (Stanford Univ, Applied Physics) for fruitful discussion. FJW would like to thank Cheng-Yu Song (National Center for Electron Microscopy, Lawrence Berkeley National Laboratory) for technical assistance. This research was supported by the Office of Naval Research (N00014-06-1-0452) and the National Science Foundation (0604277). The Advanced Light Source is supported by the Director, Office of Science, Office of Basic Energy Sciences, of the U.S. Department of Energy under Contract No. DE-AC02-05CH11231.

References

- [1] D. C. Johnston, H. Prakash, W. H. Zachariassen, and R. Viswanathan, *Materials Research Bulletin* **8**, 777 (1973).
- [2] D. C. Johnston, *Journal of Low Temperature Physics* **25**, 145 (1976).
- [3] L. J. Dejongh, *Physica C* **152**, 171 (1988).
- [4] M. R. Harrison, P. P. Edwards, and J. B. Goodenough, *Journal of Solid State Chemistry* **54**, 136 (1984).
- [5] E. Moshopoulou, P. Bordet, J. J. Capponi, C. Chaillout, B. Souletie, and A. Sulpice, *Journal of Alloys and Compounds* **195**, 81 (1993).
- [6] E. Moshopoulou, P. Bordet, A. Sulpice, and J. J. Capponi, *Physica C* **235**, 747 (1994).
- [7] J. H. Lin, T. H. Lin, and C. W. Chu, *Journal of Low Temperature Physics* **58**, 363 (1985).
- [8] R. N. Shelton, D. C. Johnston, and H. Adrian, *Solid State Communications* **20**, 1077 (1976).

- [9] W. Prellier, A. M. Haghiri-Gosnet, B. Mercey, P. Lecoeur, M. Hervieu, C. Simon, and B. Raveau, *Applied Physics Letters* **77**, 1023 (2000).
- [10] G. G. N. Angilella, G. Balestrino, P. Cermelli, P. Podio-Guidugli, and A. A. Varlamov, *The European Physical Journal B* **26**, 67 (2002).
- [11] S. Autier-Laurent, B. Mercey, D. Chippaux, P. Limelette, and C. Simon, *Physical Review B* **74**, 195109 (2006).
- [12] M. Henzler, *Surface Science* **358**, 809 (1996).
- [13] J. Z. Wu, P. Y. Hsieh, A. V. McGuire, D. L. Schmidt, L. T. Wood, Y. Shen, and W. K. Chu, *Phys. Rev. B* **44**, 12643 (1991).
- [14] H. U. Habermeier, *Journal of Superconductivity* **13**, 871 (2000).
- [15] T. Inukai, T. Murakami, and T. Inamura, *Thin Solid Films* **94**, 47 (1982).
- [16] T. Inukai and T. Murakami, *Thin Solid Films* **128**, 275 (1985).
- [17] G. Hu, V. G. Harris, and Y. Suzuki, *IEEE Transactions on Magnetics* **37**, 2347 (2001).
- [18] W. Eerenstein, T. T. M. Palstra, T. Hibma, and S. Celotto, *Phys. Rev. B* **66**, 201101 (2002).
- [19] D. T. Margulies, F. T. Parker, M. L. Rudee, F. E. Spada, J. N. Chapman, P. R. Aitchison, and A. E. Berkowitz, *Physical Review Letters* **79**, 5162 (1997).
- [20] F. C. Voogt, T. T. M. Palstra, L. Niesen, O. C. Rogojanu, M. A. James, and T. Hibma, *Phys. Rev. B* **57**, R8107 (1998).
- [21] M. Dalton and M. Kurmoo, *Synthetic Metals* **71**, 1623 (1995).
- [22] P. M. Lambert, M. R. Harrison, and P. P. Edwards, *Journal of Solid State Chemistry* **75**, 332 (1988).

- [23] H. Zheng, J. Wang, S. E. Lofland, Z. Ma, L. Mohaddes-Ardabili, T. Zhao, L. Salamanca-Riba, S. R. Shinde, S. B. Ogale, F. Bai, et al., *Science* **303**, 661 (2004).
- [24] R. V. Chopdekar, G. Hu, A. C. Ford, and Y. Suzuki, *Journal of Electronic Materials* **33**, 1254 (2004).
- [25] T. Inukai, T. Murakami, and T. Inamura, *Japanese Journal of Applied Physics* **20**, L681 (1981).
- [26] F. C. Xu, Y. C. Liao, M. J. Wang, C. T. Wu, K. F. Chiu, and M. K. Wu, *Journal of Low Temperature Physics* **131**, 569 (2003).
- [27] R. G. Buckley, B. P. Clayman, and J. C. Mikkelsen, *Physical Review B* **26**, 6509 (1982).
- [28] I. Abrahams, P. G. Bruce, W. I. F. David, and A. R. West, *Journal of Solid State Chemistry* **78**, 170 (1989).
- [29] A. T. Young, J. Feng, E. Arenholz, H. A. Padmore, T. Henderson, S. Marks, E. Hoyer, R. Schlueter, J. B. Kortright, V. Martynov, et al., *Nuclear Instruments and Methods in Physics Research Section A* **467**, 549 (2001).
- [30] P. Nachimuthu, J. H. Underwood, C. D. Kemp, E. M. Gullikson, D. W. Lindle, D. K. Shuh, and R. C. C. Perera, *AIP Conference Proceedings: Eighth International Conference on Synchrotron Radiation Instrumentation* **705**, 454 (2004).
- [31] F. M. F. de Groot, J. Faber, J. J. M. Michiels, M. T. Czyzyk, M. Abbate, and J. C. Fuggle, *Physical Review B* **48**, 2074 (1993).
- [32] F. M. F. de Groot, M. O. Figueiredo, M. J. Basto, M. Abbate, H. Petersen, and J. C. Fuggle, *Physics and Chemistry of Minerals* **19**, 140 (1992).

- [33] M. Abbate, F. M. F. de Groot, J. C. Fuggle, A. Fujimori, Y. Tokura, Y. Fujishima, O. Strelbel, M. Domke, G. Kaindl, J. van Elp, et al., *Physical Review B* **44**, 5419 (1991).
- [34] W. Ra, M. Nakayama, H. Ikuta, Y. Uchimoto, and M. Wakihara, *Applied Physics Letters* **84**, 4364 (2004).
- [35] L. A. Bugaev, A. P. Sokolenko, H. V. Dmitrienko, and A.-M. Flank, *Phys. Rev. B* **65**, 024105 (2001).
- [36] C. P. Sun, J. Y. Lin, S. Mollah, P. L. Ho, H. D. Yang, F. C. Hsu, Y. C. Liao, and M. K. Wu, *Physical Review B* **70**, (2004).
- [37] F. Gomory, *Superconductor Science and Technology* **10**, 523 (1997).
- [38] Y. Ueda, T. Tanaka, K. Kosuge, M. Ishikawa, and H. Yasuoka, *Journal of Solid State Chemistry* **77**, 401 (1988).
- [39] M. Steinbruck and A. Feltz, *Journal of Materials Science Letters* **11**, 216 (1992).
- [40] M. R. Harrison, P. P. Edwards, and J. B. Goodenough, *Philosophical Magazine Part B* **52**, 679 (1985).
- [41] D. P. Norton, D. H. Lowndes, S. J. Pennycook, and J. D. Budai, *Physical Review Letters* **67**, 1358 (1991).
- [42] N. Werthamer, E. Helfand, and P. Hohenberg, *Physical Review* **147**, 295 (1966).
- [43] S. Foner and J. McNiff, E. J., *Solid State Communications* **20**, 995 (1976).